Wetting translucency of graphene on plasmonic nanohole arrays

Wetting Translucency of Graphene on Plasmonic Nanohole Arrays

Syed Mohammad Abid Hasan[1, ‡], Nishir Mehta[1, ‡], Robin L McCarley[2], Michael M. Khonsari[1],

Manas Ranjan Gartia [1,]*

[1]*Department of Mechanical and Industrial Engineering, Louisiana State University, Baton Rouge, Louisiana 70803, United States*

[2]*Department of Chemistry, Louisiana State University, Baton Rouge, Louisiana 70803, United States*

KEYWORDS: *Plasmonic nanohole array, graphene, surface energy, contact angle*

ABSTRACT

Graphene- a carbon allotrope with atoms arranged in monolayer two-dimensional hexagonal lattice- exhibits wide range of applications in batteries, supercapacitors, solar cells, biosensing, light-emitting diodes, semi-conductors, materials composites, and coatings to name a few. Significant progress has been made to understand the electronic, mechanical, and optical characteristics of graphene. However, the wettability of graphene, which is important for surface modification and thermal/fluidic properties, is still not well understood. The level of transparency to van der Waals forces, chemical bonds, and electrostatic interactions between

1

atoms and molecules on two sides of graphene single layer is partially known. Static contact angle between the edge of sessile drop and functionalized surface provides surface tension value based on Owens-Wendt model and is important for wettability studies. In this work, we investigate the surface energy of glass, silicon wafer, and plasmonic nano-hole arrays (Silver, Polymer and Gold) suspended with CVD grown and transferred single layer of graphene. Our experimental results demonstrate that graphene is wetting transparent in the case of silicon and wetting opaque when deposited on the glass. The plasmonic nanohole arrays (NHAs) fall in the partially wetting transparent category. On plasmonic NHAs, the surface energy value got reduced with the suspending single layer graphene compared to absence of graphene. These results showed that the underlying substrate does affect the wettability of graphene monolayer due to van der Waal hydrocarbon, metal-carbide, and silica-carbon bonding which tends to provide deeper understanding of the wetting dynamics. This study elucidates the mechanism of short-range forces between water-graphene-substrate which is important during the fabrication of adhesives and coatings with controlled fluidic and heating properties.

INTRODUCTION

Understanding the interface between graphene and water is important in many applications such as water filtration[1], energy storage[2], biosensing[3] , microfluidics[4] , electronics[5] , and surface coating[6] that utilizes graphene as an active material. The wetting behavior of graphene[7] has been controversial in terms of wetting transparency[8] , wetting opacity, and wetting translucency[9]. Interestingly, all these results are also supported by molecular dynamics simulations[8] that provide insight into the effect of choice of water-carbon interaction potentials. Recent studies also point to major role of airborne particles contamination effect in the wetting experiments of graphene[10]. The wetting transparency means the wetting behavior

of graphene on substrate will follow the wetting properties of substrate ($\theta_{GS} = \theta_S$), where θ_{GS} is

the water contact angle of substrate with graphene and θ_S is the water contact angle of substrate

without graphene. The wetting opacity means the wetting properties of graphene on substrate is

independent of wetting properties of underlying substrate (e.g., $\theta_{GS} = constant = 90^o$). The

wetting translucency models take into account the detailed mechanism of van der Waals (vdW)

interaction between water-graphene and water-substrate[9]. Such models argue that dominance

of vdW interaction force will decide if the graphene on substrate will be wetting transparent or

wetting opaque. It also showed that the wetting transparency is generally valid within the water

contact angle range of $30 < \theta < 90$ and breaks down for super hydrophilic or super

hydrophobic surfaces[8]. For example, $\theta_{G+S} = \theta_G + \theta_S$ and $\gamma(1 + cos\varphi) = -\theta_{G+S}$. If $|\theta_G| <<$

$|\theta_S|$, then $cos\theta \propto |\theta_S|$ and hence contact angle will be decided by the substrate, i.e. graphene will

be wetting transparent. Conversely, if $|\theta_G| >> |\theta_S|$, then $cos\theta \propto |\theta_G|$ and the contact angle will

be decided by graphene; hence, graphene is opaque to wetting.

While most analyses aiming to understand the wetting behavior of graphene are based on contact

angle measurements, Kozbial et al. focused on the surface energy calculation and found that

surface energy starts to decrease when airborne contamination exist[11]. Annamalai et al.

calculated the surface energy and contend that van der Waal force mediates wettability on

intrinsic dispersive surface of CVD grown graphene and other 2D materials[12].

Interfacial interactions are primarily governed by the surface energy. For example, a liquid with

low surface energy (e.g. water surface energy/surface tension is 72.8 mJ/m^2) tends to spread on a

substrate with high surface energies in order to minimize the total surface energies. General

methods of increasing surface energies are oxygen plasma treatment, chemical etching, and sand

blasting. These surface activation methods increase the surface energy and make the surface

hydrophilic. Conversely, passivation methods like waxing, sialyation, hydro-generation lowers the surface energy, and make the surface non-wetting or hydrophobic.

Many mathematical models are available to determine unknown interfacial energy in Young's equation. Hejda et al.[13] compared various approaches of calculating surface energy such as Zisman's approach[14], Owens and Wendt[15] geometric mean method, harmonic mean method developed by Wu, acid-base theory formulated by van Oss et al[16], and equation of state approach by Neumann et al[17] . In this work, surface energy of the substrates coated with and without graphene is calculated using the Owens and Wendt (OW) model. We utilized the static wetting contact angles measured using water (polar liquid) and diiodomethane (non-polar) liquid sessile drop to calculate the surface energy. Additionally, we used ethylene glycol and formamide along with water and diiodomethane to obtain the contact angles for calculating the surface energy.

Although a number of studies of contact angle measurement on graphene has been reported, only few have analyzed the surface energy of graphene[11]. Previously nanostructured coated graphene structure have been utilized for Surface Enhanced Raman Spectroscopy (SERS) studies[18]. However, detailed analysis of interface surface energy analysis which takes into consideration polar and non-polar behavior of the surface under investigation along with the consideration of time-limiting droplet evaporation is lacking in the available literature.

Nano hole arrays based devices have been utilized in various fields such as NHA sensors, plasmonic biosensors, opto-fluidic elements with NHA, NHA based chemical analysis and so on[19]. But, the report of surface energy of graphene on nanostructured plasmonic surfaces are scarce. Here we report the surface energy analysis of metal coated nanostructured polymer surface suspended with graphene. Further, we have performed a parametric study to understand

4

the dependence of surface energy on the polar and non-polar component of static contact angle (in the range 0-180°).

Figure 1 shows the optical and scanning electron microscopy (SEM) images of graphene suspended nanohole array (NHA) structures. NHA with two different depth of the holes (h = 250 nm, 1000 nm) are shown. Both the devices have hole diameter, d = 180 nm, and pitch, p = 350 nm, and holes are arranged in square arrays. Experiments were performed with two different plasmonic materials (Au, Ag) deposited on the NHA (thickness, t = 90 nm). For comparison, a single layer graphene (SLG) on Si (Figure 1c), glass, and NHA without metal coating (Figure 1l) was utilized. The optical images of Au coated h = 250 nm devices are shown in Figure 1f, g. The corresponding SEM images are shown in Figure 1e (top view) and Figure 2c-f (cross-sectional view). The optical images of Au coated h = 1000 nm devices are shown in Figure 1h, k. The corresponding SEM images are shown in Figure 1d, i, j (top view) and Figure 2a, b (cross-sectional view). The optical images of Ag coated h = 1000 nm devices are shown in Figure 1b and the corresponding top view SEM images are shown in Figure 1m. The darker flakes in the SEM (Figure 1, 2) and optical image indicate presence of rotational disorder between domains and grain boundaries in a self-limiting growth of monolayer graphene. Wrinkles shown in the Figure 2a, c originate due to mismatch in the coefficient of thermal expansion between the graphene and copper (Cu) substrate. A gold coated surface without graphene appears bright due to the increased secondary electrons emission. The surface covered with graphene has decreased the secondary electron emission due to the increase in the penetration depth as well as due to the presence of low-energy chemical bonds between the graphene and substrate. Drop in transmission spectra was observed to be approximately 2.3% when the graphene was deposited on a glass substrate which in turn corresponds to monolayer of graphene (Figure S1).

5

Transmission drop is small due to linear dispersion of electrons similar to bandstructure of light and unlike parabolic dispersion in traditional 2-D materials. In order to confirm the presence of single layer graphene (SLG) on the devices, Raman spectroscopy experiments were performed. The sample on NHA (Figure S2) showed the D peak at 1322 cm^{-1}, G peak at 1590 cm^{-1}, and 2D peak at 2635 cm^{-1}. Lorentzian curve with FWHM of approximately 39 cm^{-1} was obtained while measuring two-dimensional band structure of graphene which signifies single layer of graphene.

The shift in the Fermi level of graphene can be inferred from the direction of the shift in graphene 2D peak. A redshift in the 2D peak is associated with an upward movement of the Fermi level, and a blueshift in the 2D peak is associated with downward movement of the Fermi level. The upward movement of Fermi levels are linked to doping by electrons, while the downward movement of Fermi levels are generally linked to hole doping[20, 21] . Since the 2D peak is blue-shifted, the graphene on NHAs are p-doped. This line of reasoning is also supported by previous literature data of adatom formation of graphene with Au nanoparticles[22-24]. The increase in the FWHM of the G peak on NHA (FWHM = 47 cm^{-1}) compared to graphene on glass substrate (FWHM = 18 cm^{-1}) is another evidence of decrease in electron concentration and formation of p-doped graphene[25, 26].   In the p-type dopant for graphene, the highest occupied molecular orbital (HOMO) level is situated below the Fermi level of graphene (Figure S3). This is reasonable as the work function of graphene is ~ 4.5 eV [27, 28], whereas the work function of Au is ~ 5.5 eV and that of Ag is ~ 4.26 – 4.6 eV [29, 30]. Hence, electron transfer from graphene to Au is expected.

The formation of p-doped surface leads to hydrophilic surfaces [31] . This is because the negatively charged oxygen atoms of the water molecule will be attracted by the positively charged (due to the p-type doping) graphene surfaces. It should be noted that the resultant force

6

will be dependent on the Coulomb force and the van der Waals force. The net outcome of this

resultant force is the increase in the density of states of either electrons or holes leading to a

hydrophilic surface [32] . Another evidence of charge transfer and formation of complex π-π

bond between metal and graphene layer is revealed by examination of the XPS results. At the

interfacial region of water and graphene several noncovalent interactions such as van der Waals

interaction, electrostatic interactions (coulombic)[33], hydrogen bonding, and π-π stacking

interactions[34] are possible. The π-π interaction between the interfaces of graphene and water

interfaces plays an important role as the oxygen lone pair of water tends to interact with the π-

electron cloud of the graphene surface. Don et al. [35] discussed this interaction in details. In the

paper, the authors have calculated the noncovalent interactions energy of graphene-like structure

(Coronene) with water. They reported that the individual magnitudes of electrostatic (coulombic)

(~ -3.75 kcal/mol), exchange (~ +8.5 kcal/mol), and dispersion (~ -5.75 kcal/mol) terms are high,

but the sum of these terms essentially balance each other (~ -1 kcal/mol), leaving the many-body

interaction energy terms like charge transfer and induction energy to be important at the

interface. At the interface, there is competing interaction between carbon (of graphene) with O or

H of water and water – hydroxyl (of substrate) interaction. When we have nanohole array

plasmonic substrate (e.g. Ag NHA or Au NHA), the substrate comprises of lots of free electrons.

Now the electron clouds of plasmonic substrate will interact with the electron cloud of graphene

(π-π electrons). This will lead to reduction in the interaction energy of graphene with water.

Figure 3e shows the high-resolution C 1s XPS results of graphene on different substrate. The

deconvolution of the spectra and the peak fittings are provided in Figure S4. The sp2 carbon

(C=C) can be assigned to peaks at 284.2-284.5 eV (found for graphene on glass, Si and polymer

NHA). The higher energy peaks at 287.3 – 288.6 eV are generally assigned to O-C=C [36].

Generally, sp2 bonding has a lower binding energy than the sp3 bonding (due to the presence of relatively easily polarizable π-electrons; for example C-C has binding energy of ~285.2 eV). Hence, the peaks at 283.2 and 283.6 eV for Ag NHA and Au NHA respectively, could be attributed to formation of more π-π bond between metal and graphene layer.

To provide further evidence of charge transfer between graphene and metal surfaces on the plasmonic substrate, transmission spectra was collected for the Au NHA. Figure 3f shows the transmission spectra of h = 250 nm Au NHA device and Figure 3g shows the transmission spectra of h = 1000 nm device with (red curve) and without (black curve) graphene on it. With the graphene layer, the resonance peak wavelength shifted by 2 nm (h = 250 nm) and by 19 nm (h = 1000 nm). The corresponding electromagnetic field on the NHA device (h = 1000 nm) is shown in Figure 4c, d. The device will support electromagnetic field enhancement of at least 10^4 (Figure 4d, using the typical electromagnetic field enhancement model of enhancement factor, $EF \propto |E|^4$)[18] .

To demonstrate the electromagnetic field enhancement on the plasmonic substrate, we have performed Raman mapping (Figure 4a) of graphene layer on top of the Au NHA (h = 1000 nm) device. The device is covered with water on half of the surfaces (as shown in the inset of Figure 4a). The Raman map is shown for the graphene 2D peak at ~ 2640 cm^{-1}. Figure 4b shows the Raman spectra at different positions on the plasmonic device (the identification of corresponding positions are in Figure S5). As shown in Figure 4a, b, the presence of water on top of the graphene further enhanced the interaction between graphene and the underneath plasmonic substrate leading to enhancement in Raman scattering. Previously, we demonstrated that the water layer enhances both the excitation electromagnetic field and the emitted spontaneous

8

radiation field due to increase in the optical density of states near the metal – graphene interface

[18] .

Surface Energy Calculation

Next, we proceed to calculate the modification in the surface energies leading to change in water

contact angles on the plasmonic substrate due to the above mentioned graphene-substrate

interactions. The surface energies for different samples were measured based on the static water

contact angle measurements. Owens –Wendt – Rabel - Kaelbel (OWRK) model was used to

measure the surface energy with four liquids, namely water, ethylene glycol, formamide and

diiodomethane, for which the polar and dispersive surface energy components were known

(Table S1). Figure S6 shows the schematic of different contact angles made by a liquid droplet

kept on a surface. The wetting phenomena illustrating in this diagram can explained by

Young's[37] equation as follows:

$$\gamma_{lv}\cos\theta = \gamma_{sv} - \gamma_{sl} \tag{1}$$

where θ is the contact angle, γ_{sl} is the free energy associated with the solid and liquid interface,

γ_{lv} is the free energy at the liquid and vapor interface, and γ_{sv} is the free energy of the solid

surface. The free energy of the solid surface can be measured utilizing the OWRK model which

requires two liquids and their polar and dispersive component of surface free energy. The

equation reduces to the following form:

$$\gamma_{sl} = \gamma_{sv} + \gamma_{lv} - 2\left(\sqrt{\gamma_{sv}^d\gamma_{lv}^d} + \sqrt{\gamma_{sv}^p\gamma_{lv}^p}\right) \tag{2}$$

where γ_{sv}^d and γ_{lv}^d are the dispersive components; γ_{sv}^p and γ_{lv}^p are the polar components of the free

energy of the solid and free energy between liquid and vapor interface, respectively. From

9

equation (1) and (2) the following equation can be developed to represent a linear equation of a straight line of the form, $y = mx + C$,

$$\sqrt{\gamma_{sv}^d} + \sqrt{\gamma_{sv}^p}\sqrt{\frac{\gamma_{lv}^p}{\gamma_{lv}^d}} = \frac{1}{2}\frac{\gamma_{lv}(1 + \cos\theta)}{\sqrt{\gamma_{lv}^d}} \qquad (3)$$

where y $= \frac{1}{2}\frac{\gamma_{lv}(1 + \cos\theta)}{\sqrt{\gamma_{lv}^d}}$, $m = \sqrt{\gamma_{sv}^p}$, $x = \sqrt{\frac{\gamma_{lv}^p}{\gamma_{lv}^d}}$, $C = \sqrt{\gamma_{sv}^d}$.   (4)

Finally, $\gamma_{sv} = \gamma_{sv}^d + \gamma_{sv}^p$ (5)

However, we would like to emphasize one of the terms from equation 3, $\gamma_{lv}(1 + \cos\theta)$, which estimates the work of adhesion. This term is often expressed as W_{SL}[38]. As the thermodynamic contact angle is unknown, the calculated surface energy using Young-Dupre equation may lead to error [39]. Nevertheless, there are some direct methods for calculating this term from the work of separation such as falling drop weight technique [39]. By knowing the polar and dispersive components of the four liquids, we calculated the free energy of the solid surface. By measuring the contact angle on different substrates (θ) for water, ethylene glycol, formamide and diiodomethane (Table S3, S4), and using the value of liquid surface energies from Table S1, the value of y and x can be plotted (Figure S7, S8). We also measured the surface energies based on water and diiodomethane and Figure S7 is showing plot from where we got the values of x and y to determine surface energies. The linear fit to the experimental data provides the value of m and C. Having the dispersive and polar component of surface energies at the solid-air interface for each substrate, the surface energy of the substrate was calculated using equation (5). The calculated values of surface energies on different substrate in the presence and absence of graphene is provided in Table S2. Typical water contact angle values for different substrates without (gray color) and with (blue color) graphene layer are plotted in Figure S9. It shows that the graphene layer over the substrate is wetting transparent if the water contact angle of the

10

supporting substrate lies in the range $30^o < \theta < 90^o$ (for example, Si, Cu, Au). However, if $\theta <$

30° (e.g. glass, oxygen plasma (OP) treated SiO_2), the contact angle increases with graphene

layer compared to bare substrate. Similarly, when $\theta > 90^o$ (e.g. silane (octadecyltrichlorosilane

or OTS) treated SiO_2, SiO_2 nanoparticles), the contact angle decreases with the addition of

graphene layer. In Figure 5a, we have shown the histogram for contact angles with respect to

water for different substrates with and without graphene. As shown in Figure 5b, we calculated

the variation of surface energies with graphene layer on top of the NHAs. For comparison, the

surface energies without the graphene layer is also plotted. Figure 5b shows that the surface

energies have decreased for all of the nanohole arrays devices with the addition of graphene.

This is interesting as all the samples except Ag NHA, have their water contact angles in the

range of $30^o < \theta < 90^o$ (Figure 5d). To explain the transparency of graphene layer, Figure 5c

illustrate the relation between the contact angle with graphene (θ_{GS}) and without graphene layer (

θ_S). The wetting transparency line (dotted line) exhibits the criteria where $\theta_{GS} = \theta_S$. Along with

our experimental results based on polar (water) and nonpolar (diiodomethane) liquids and

literature values for different substrates in Figure 5c suggest that the wetting transparency of

graphene is dependent on the polarity of the liquid used and the presence of any charge transfer

between substrate and graphene layer. It should also be noted that the water transparency does

not mean that the surface energies are equal. For example, h = 250 nm Au NHA has quite similar

water contact angles with and without graphene. However, the surface energies of the same

device is different as the contact angle of diidomethane is not the same on h = 250 nm Au NHA

with and without graphene (Figure 5b, d). To understand the changes in surface energy while

changing the contact angles, we performed parametric studies by changing the water contact

angles (Figure S10) and diidomethane (Figure S11) contact angles in the range of 0-180º. The

general trend for all the devices (including plasmonic NHAs) is that when the water contact angle becomes greater in the range of $0^o < \theta < 90^o$, the surface energies decreases. On the other hand, within the range of $90^o < \theta < 180^o$, the surface energy increases when the water contact angle becomes greater. The water contact angle of $\theta = 180^o$ showed the highest surface energies and the surface energies decreases with the increase of diiodomethane contact angle with the substrate (Figure S10). The same trend is observed when the liquid used is nonpolar (with some exception such as glass and Ag NHA).

In conclusion, we observed wetting translucency behavior of graphene on the nanoplasmonic substrate. As nanoplasmonics deals with the optical phenomena of metal surfaces at nanoscale range so this finding would be very much helpful for future application. The wetting behavior of graphene is effected by the supporting substrate depending on extend of charge transfer and π-plasmon interactions. The wetting behavior of graphene depends on the polarity of liquid. Finally, the surface energies of graphene on the nanoplasmonic substrate is lower compared to the surface energies of bare substrate.

MATERIALS AND METHODS

Graphene synthesis

Monolayers of graphene were grown using chemical vapor deposition (CVD) technique on Cu substrates due to low solubility of C atoms in Cu. Cu substrate acted as the active catalyst to promote surface reaction and nucleation of graphene layer by lowering the energy barrier for the reaction when the mixture of CH_4-H_2 is passed over the substrate. Polymethyl methacrylate (PMMA) was used for the transfer of graphene. PMMA was deposited on the one side of graphene grown on Cu substrate and baked to evaporate solvents. Metal etchants O_2 plasma and

FeCl₃ were used to remove copper and cleaning was done via deionized water. Combination of

remaining graphene attached to PMMA scaffold was wet transferred to surfaces analyzed in this

study. In the final step, PMMA was dissolved using methanol and dichloromethane solution.

Contact angle measurements

A 1000 µL sessile drop is casted via computer controlled micro-syringe positioned above on the

solid surface of the sample under investigation on a Kruss-Scientific system. Stage is manually

controlled via rack-and-pinion drive and adjusted based on baseline match with software

contour. An image of the static drop of both polar and non-polar liquid is recorded with the high-

speed machine vision camera as shown in Figure S12 and then processed using drop shaping

analysis software. Contact angles are measured at the three-phase point of contact on a sessile

droplet profile in the equilibrium state (Figure S13) with the well-defined vibration insulation of

the optical subsystems. All the measurements were captured within 1 minute of liquid drop-

casting because as shown in Figure S13, water evaporation at the room temperature significantly

factors in with the progression of time. In the case of diiodomethane, effect of evaporation is

negligible. After recording the water contact angle, substrates were sufficiently exposed to

heated environment dried for prolonged time (approximately 25-30 minutes) in order to

evaporate the residual water. The heating temperature was kept well below the melting

temperature of the polymer. The dynamic contact angle measurements are shown in Figure S14.

Further, Table S5 compares the results obtained from static and dynamic measurements.

Raman and X-ray photoelectron spectroscopy measurements

Raman signal measurements were done using 532 nm Nd:YAG laser in a Renishaw PL/Raman

micro-spectroscopy system. Raman signals from the graphene coated samples were collected via

13

50x long working distance objective in the wavenumber range of 200 to 3000 cm^{-1}. X-ray

Photoelectron Spectroscopy results were obtained using high performance Kratos AXIS 165

XPS/AES instrument.

SEM Imaging

Environmental scanning electronic microscope JSM-6610 LV was used to capture the wetting

images of substrate with nanohole arrays at 10 kV in the low-pressure chamber shown in Figure

1. Graphene coated substrates were analyzed in secondary electron beam mode in SEM by tilting

the substrates at 52 degrees and at 0 degrees. Cross-section images were taken by cutting the

substrate via focused ion beam with current less than 1 pA to prevent polymer melting.

ASSOCIATED CONTENT

Supporting Information

AUTHOR INFORMATION

Corresponding Author

*E-mail: mgartia@lsu.edu

Author Contributions

The manuscript was written through contributions of all authors. All authors have given approval

to the final version of the manuscript. ‡These authors contributed equally.

Notes

The authors declare no competing financial interest.

1
2
3
4
5
6
7
8
9
10
11
12
13
14
15
16
17
18
19
20
21
22
23
24
25
26
27
28
29
30
31
32
33
34
35
36
37
38
39
40
41
42
43
44
45
46
47
48
49
50
51
52
53
54
55
56
57
58
59
60

ACKNOWLEDGMENTS

REFERENCES

1.   Suk ME, Aluru N. Water transport through ultrathin graphene. The Journal of Physical Chemistry Letters. 2010;1(10):1590-4.

2.   Zhu J, Yang D, Yin Z, Yan Q, Zhang H. Graphene and graphene-based materials for energy storage applications. Small. 2014;10(17):3480-98.

3.   Wu L, Chu H, Koh W, Li E. Highly sensitive graphene biosensors based on surface plasmon resonance. Optics express. 2010;18(14):14395-400.

4.   He RX, Lin P, Liu ZK, Zhu HW, Zhao XZ, Chan HL, et al. Solution-gated graphene field effect transistors integrated in microfluidic systems and used for flow velocity detection. Nano letters. 2012;12(3):1404-9.

5.   Li X, Zhu Y, Cai W, Borysiak M, Han B, Chen D, et al. Transfer of large-area graphene films for high-performance transparent conductive electrodes. Nano letters. 2009;9(12):4359-63.

6.   Prasai D, Tuberquia JC, Harl RR, Jennings GK, Bolotin KI. Graphene: corrosion-inhibiting coating. ACS nano. 2012;6(2):1102-8.

7.   N'guessan HE, Leh A, Cox P, Bahadur P, Tadmor R, Patra P, et al. Water tribology on graphene. Nature communications. 2012;3:1242.

8.   Rafiee J, Mi X, Gullapalli H, Thomas AV, Yavari F, Shi Y, et al. Wetting transparency of graphene. Nature materials. 2012;11(3):217.

9.   Shih C-J, Strano MS, Blankschtein D. Wetting translucency of graphene. Nature materials. 2013;12:866-9.

10.   Li Z, Wang Y, Kozbial A, Shenoy G, Zhou F, McGinley R, et al. Effect of airborne contaminants on the wettability of supported graphene and graphite. Nature materials. 2013;12(10):925.

11.   Kozbial A, Li Z, Conaway C, McGinley R, Dhingra S, Vahdat V, et al. Study on the surface energy of graphene by contact angle measurements. Langmuir. 2014;30(28):8598-606.

12.   Annamalai M, Gopinadhan K, Han SA, Saha S, Park HJ, Cho EB, et al. Surface energy and wettability of van der Waals structures. Nanoscale. 2016;8(10):5764-70.

13.   Hejda F, Solar P, Kousal J, editors. Surface free energy determination by contact angle measurements–a comparison of various approaches. WDS; 2010.

14.   Fox H, Zisman W. The spreading of liquids on low energy surfaces. I. polytetrafluoroethylene. Journal of Colloid Science. 1950;5(6):514-31.

15.   Owens DK, Wendt R. Estimation of the surface free energy of polymers. Journal of applied polymer science. 1969;13(8):1741-7.

16.   Van OC, Chaudhury M, Good R. Monopolar surfaces. Adv Colloid Interface Sci. 1987;28:35-64.

16

17. Neumann A, Good R, Hope C, Sejpal M. An equation-of-state approach to determine surface tensions of low-energy solids from contact angles. Journal of colloid and interface science. 1974;49(2):291-304.

18. Mahigir A, Chang T-W, Behnam A, Liu GL, Gartia MR, Veronis G. Plasmonic nanohole array for enhancing the SERS signal of a single layer of graphene in water. Scientific reports. 2017;7(1):14044.

19. Prasad A, Choi J, Jia Z, Park S, Gartia MR. Nanohole array plasmonic biosensors: Emerging point-of-care applications. Biosensors and Bioelectronics. 2019; 130: 185-203.

20. Gupta S, Carrizosa S, Jasinski J, Dimakis N. Charge transfer dynamical processes at graphene-transition metal oxides/electrolyte interface for energy storage: Insights from in-situ Raman spectroelectrochemistry. AIP Advances. 2018;8(6):065225.

21. Wang W, Liang S, Yu T, Li D, Li Y, Han X. The study of interaction between graphene and metals by Raman spectroscopy. Journal of Applied Physics. 2011;109(7):07C501.

22. Gierz I, Riedl C, Starke U, Ast CR, Kern K. Atomic hole doping of graphene. Nano letters. 2008;8(12):4603-7.

23. Giovannetti G, Khomyakov P, Brocks G, Karpan Vv, Van den Brink J, Kelly PJ. Doping graphene with metal contacts. Physical review letters. 2008;101(2):026803.

24. Chan KT, Neaton J, Cohen ML. First-principles study of metal adatom adsorption on graphene. Physical Review B. 2008;77(23):235430.

25. Ferrari AC. Raman spectroscopy of graphene and graphite: disorder, electron–phonon coupling, doping and nonadiabatic effects. Solid state communications. 2007;143(1-2):47-57.

26.   Pinto H, Markevich A. Electronic and electrochemical doping of graphene by surface adsorbates. Beilstein journal of nanotechnology. 2014;5(1):1842-8.

27.   Liang S-J, Ang L. Electron thermionic emission from graphene and a thermionic energy converter. Physical Review Applied. 2015;3(1):014002.

28.   Song SM, Park JK, Sul OJ, Cho BJ. Determination of work function of graphene under a metal electrode and its role in contact resistance. Nano letters. 2012;12(8):3887-92.

29.   Uda M, Nakamura A, Yamamoto T, Fujimoto Y. Work function of polycrystalline Ag, Au and Al. Journal of electron spectroscopy and related phenomena. 1998;88:643-8.

30.   Akbi M, Lefort A. Work function measurements of contact materials for industrial use. Journal of Physics D: Applied Physics. 1998;31(11):1301.

31.   Melios C, Giusca CE, Panchal V, Kazakova O. Water on graphene: review of recent progress. 2D Mater. 2018;5(2):022001.

32.   Hong G, Han Y, Schutzius TM, Wang Y, Pan Y, Hu M, et al. On the mechanism of hydrophilicity of graphene. Nano letters. 2016;16(7):4447-53.

33.   Chen J, Zhou G, Chen L, Wang Y, Wang X, Zeng S. Interaction of graphene and its oxide with lipid membrane: a molecular dynamics simulation study. The Journal of Physical Chemistry C. 2016;120(11):6225-31.

34.   Karachevtsev MV, Stepanian SG, Ivanov AY, Leontiev VS, Valeev VA, Lytvyn OS, et al. Binding of polycitydylic acid to graphene oxide: spectroscopic study and computer modeling. The Journal of Physical Chemistry C. 2017;121(33):18221-33.

35.   Subasinghege Don V, David R, Du P, Milet A, Kumar R. Interfacial Water at Graphene Oxide Surface: Ordered or Disordered? The Journal of Physical Chemistry B. 2019;123(7):1636-49.

36.   Chaichi A, Wang Y, Gartia MR. Substrate Engineered Interconnected Graphene Electrodes

with Ultrahigh Energy and Power Densities for Energy Storage Applications. ACS applied

materials & interfaces. 2018;10(25):21235-45.

37.   Young T. III. An essay on the cohesion of fluids. Philosophical transactions of the royal

society of London. 1805(95):65-87.

38.   Dupré A, Dupré P. Théorie mécanique de la chaleur: Gauthier-Villars; 1869.

39.   Tadmor R, Das R, Gulec S, Liu J, E. N'guessan H, Shah M, et al. Solid–liquid work of

adhesion. Langmuir. 2017;33(15):3594-600.

LIST OF FIGURES
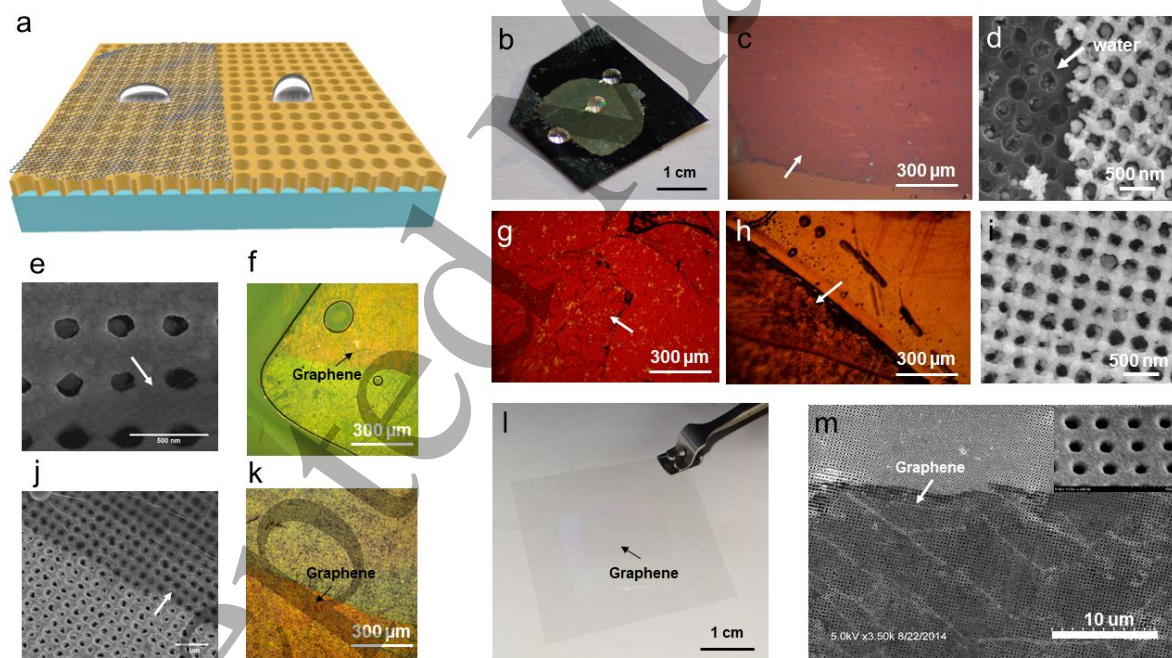
Figure 1. (a) Schematic showing water droplets over graphene monolayer suspended on plasmonic

nanohole array (NHA) substrate. (b) Optical image of water droplets on graphene coated Ag NHA.

Optical images of various substrate coated with single layer graphene (SLG) is shown for: (c) Si,

(f) Au NHA in transmission mode, (h = 250 nm), (g) Au NHA in reflection mode (h = 1000 nm),

(h) Ag NHA in reflection mode, (k) Au NHA in transmission mode (h = 1000 nm) (l) polymer

NHA. The arrow is showing the SLG. The scanning electron microscopy (SEM) images are shown

for: (d, i, j) Au NHA (h = 1000 nm), (e) Au NHA (h = 250 nm), and (m) Ag NHA. The inset of

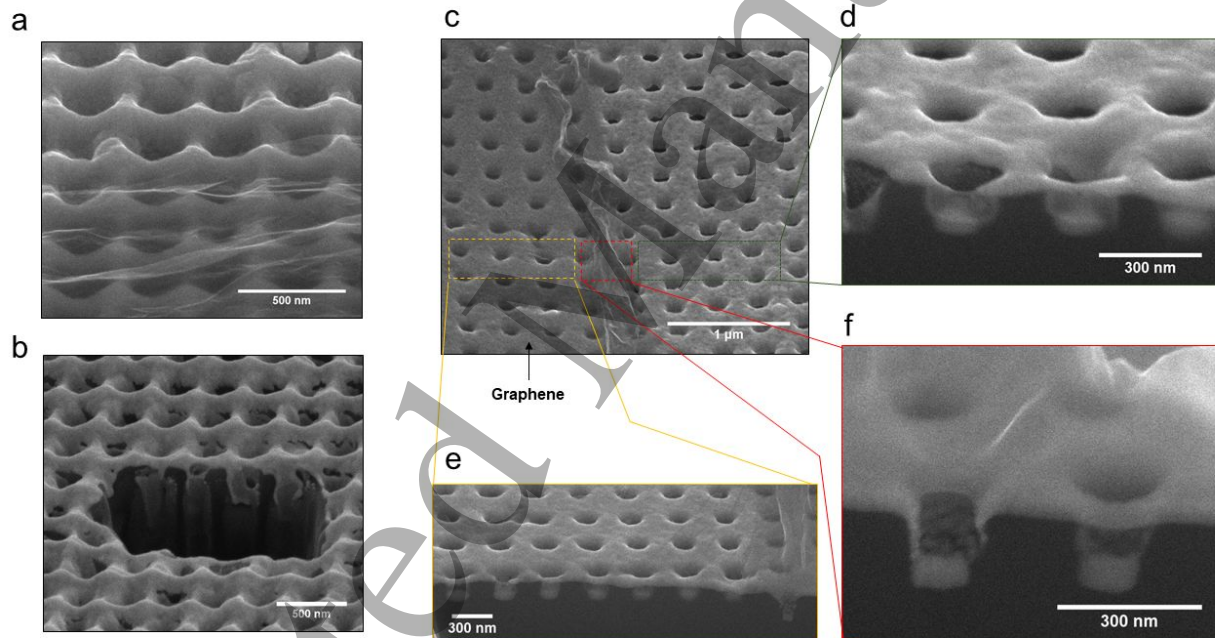(m) shows the nanoholes arranged in square arrays with pitch, p = 350 nm.

Figure 2. (a) SEM image of Au NHA (h = 1000 nm) taken at a tilt angle of 52° showing the

SLG. (b) The corresponding cross-sectional image of Au NHA (h = 1000 nm). SEM images of

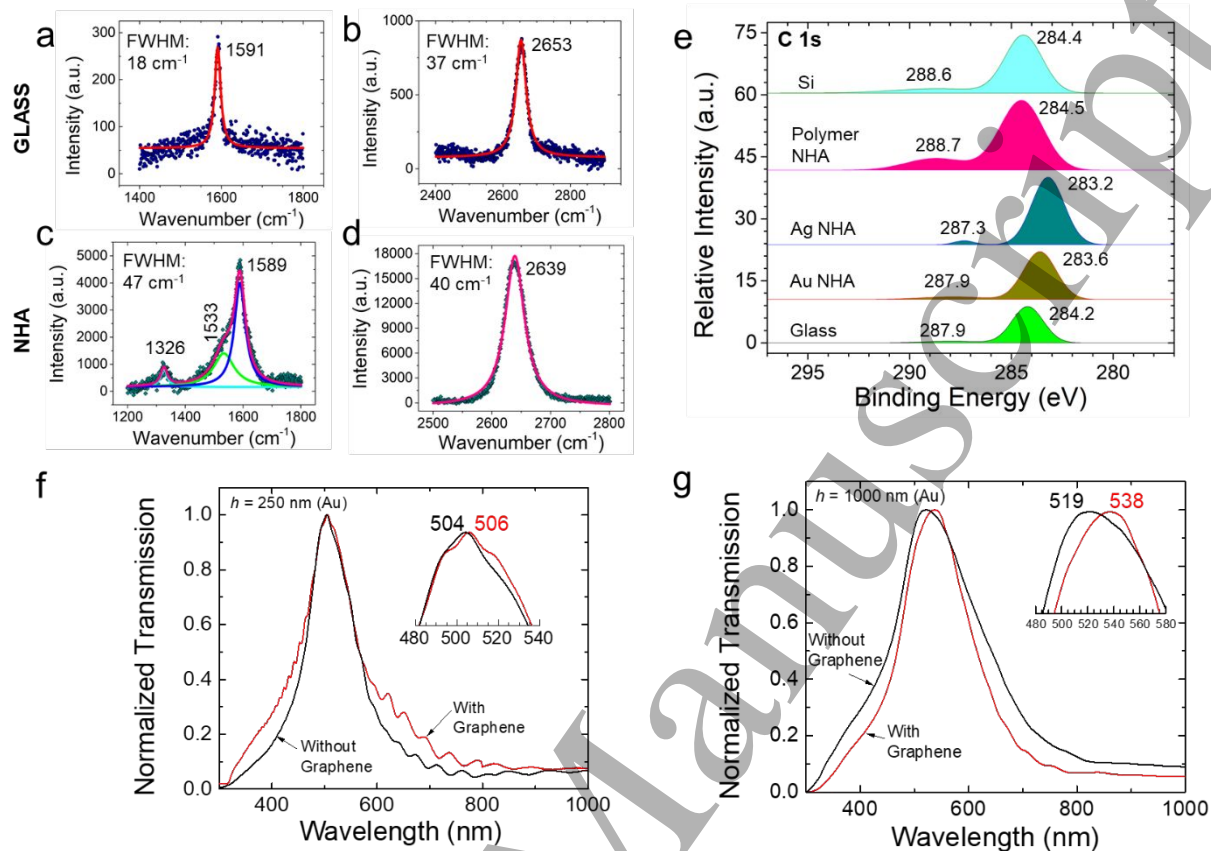Au NHA (h = 250 nm) showing the (c) top view, and (d-f) cross-sectional view.

Figure 3. (a) Comparison of Raman spectra on glass and NHA substrate for the G and 2D peaks showing the presence of SLG. (b) Comparison of XPS results for SLG on different substrate. The shift of the 'C' peaks demonstrate the π-π interaction of graphene electrons with the supporting substrate. Optical transmission peaks showing the plasmon resonance shift due to the presence of graphene monolayer over (c) Au NHA (*h* = 250 nm), and (d) Au NHA (*h* = 1000 nm).
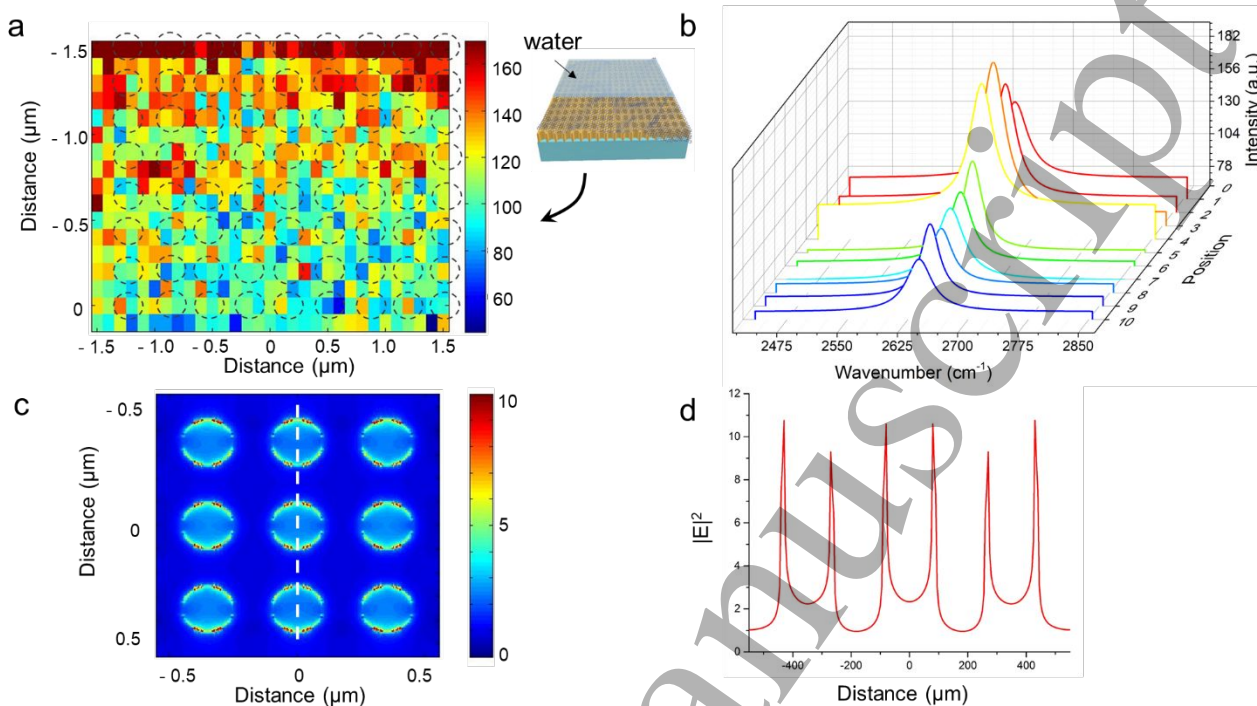
Figure 4. (a) Raman map showing the intensity distribution of graphene 2D peak over the Ag

NHA. Water layer was over the top half of the graphene coated NHA (from y = -0.75 μm to

y = -1.5 μm). The bottom half (from y = -0.75 μm to y = 0 μm) had air. The inset image shows

the experimental arrangement. (b) The corresponding Raman spectra at selected positions of the

map is plotted. The graphene layer with water on top of it showed ~ 2X higher intensity

compared to graphene without water layer over it. (c) The electromagnetic field distribution of

Ag NHA showing localized hot spot around the rim of the nanoholes. (d) The line plot showing
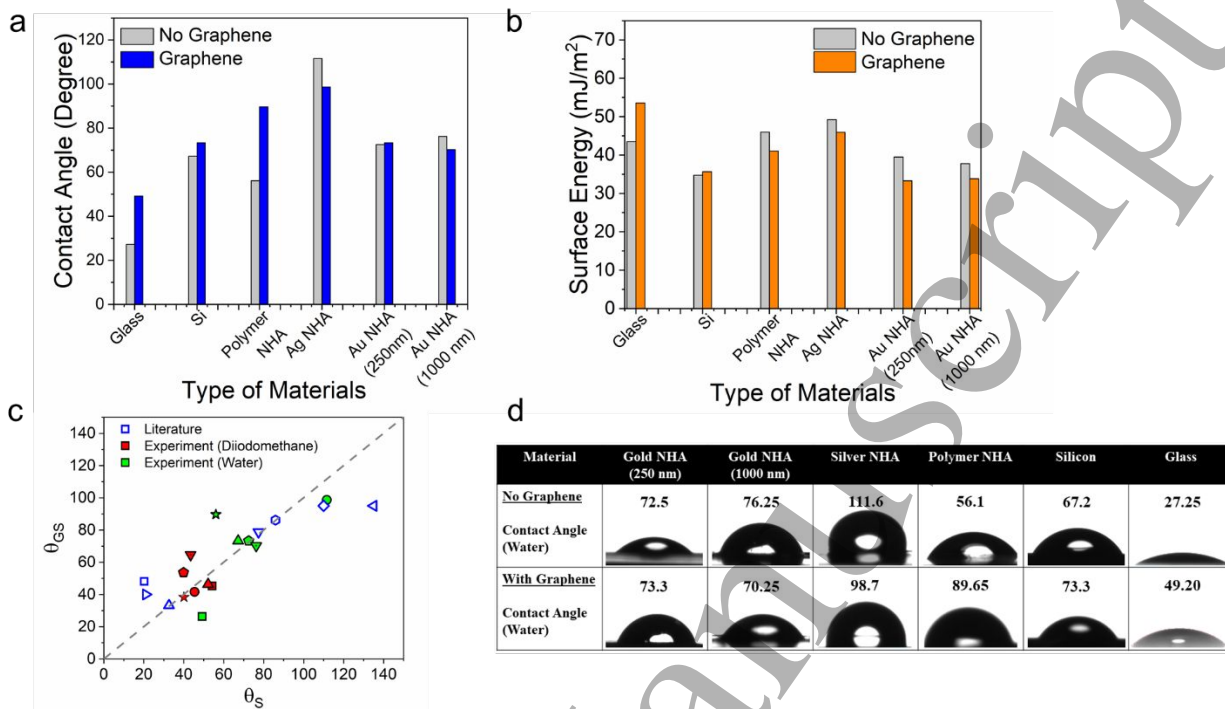
the field distribution along the dotted line in (c).

Figure 5. (a) Comparison of water contact angles of different substrates with and without graphene layer; (b) The calculated surface energies of various substrates with and without graphene layer; (c) Wetting Transparency of graphene layer on various substrates: glass (□), Ag (○), Si (Δ), h = 250 nm Au NHA(⊡), h = 1000 nm Au NHA (∇), polymer NHA (☆),OTS SiO$_2$ (◆), OP SiO$_2$ (►), and Au (▼). All the open symbols are the literature data, all the filled symbols are experimental data. The green filled symbols are contact angles with water and the red filled symbols are contact angles with diiodomethane. (d) Images showing the water contact angle measurement of different substrates with and without graphene layer.

23